

Spin transport characteristics modulated by the GeBi interlayer in $Y_3Fe_5O_{12}$/GeBi/Pt heterostructures

Mingming Li(李明明), Lei Zhang(张磊), Lichuan Jin(金立川), and Haizhong Guo(郭海中)

Citation: Chin. Phys. B, 2024, 33 (**2**): 027201. DOI: 10.1088/1674-1056/ace3aa
Journal homepage: http://cpb.iphy.ac.cn; http://iopscience.iop.org/cpb

What follows is a list of articles you may be interested in

Magnetization-direction-dependent inverse spin Hall effect observed in IrMn/NiFe/Cu/YIG multilayer structure

Runrun Hao(郝润润), Ruxue Zang(臧如雪), Tie Zhou(周铁), Shishou Kang(康仕寿), Shishen Yan(颜世申), Guolei Liu(刘国磊), Guangbing Han(韩广兵), Shuyun Yu(于淑云), Liangmo Mei(梅良模)
Chin. Phys. B, 2019, 28 (**3**): 037202. DOI: 10.1088/1674-1056/28/3/037202

Inverse spin Hall effect in ITO/YIG exited by spin pumping and spin Seebeck experiments

Kejian Zhu(朱科建), Weijian Lin(林伟坚), Yangtao Su(苏仰涛), Haibin Shi(石海滨), Yang Meng(孟洋), Hongwu Zhao(赵宏武)
Chin. Phys. B, 2019, 28 (**1**): 017201. DOI: 10.1088/1674-1056/28/1/017201

Spin-independent transparency of pure spin current at normal/ferromagnetic metal interface

Runrun Hao(郝润润), Hai Zhong(钟海), Yun Kang(康韵), Yufei Tian(田雨霏), Shishen Yan(颜世申), Guolei Liu(刘国磊), Guangbing Han(韩广兵), Shuyun Yu(于淑云), Liangmo Mei(梅良模), Shishou Kang(康仕寿)
Chin. Phys. B, 2018, 27 (**3**): 037202. DOI: 10.1088/1674-1056/27/3/037202

Spin-filter effect and spin-polarized optoelectronic properties in annulene-based molecular spintronic devices

Zhiyuan Ma(马志远), Ying Li(李莹), Xian-Jiang Song(宋贤江), Zhi Yang(杨致), Li-Chun Xu(徐利春), Ruiping Liu(刘瑞萍), Xuguang Liu(刘旭光), Dianyin Hu(胡殿印)
Chin. Phys. B, 2017, 26 (**6**): 067201. DOI: 10.1088/1674-1056/26/6/067201

Spin pumping through magnetic impurity effect

Deng Wei-Yin (邓伟胤), Sheng Li (盛利), Xing Ding-Yu (邢定钰)
Chin. Phys. B, 2015, 24 (**8**): 087202. DOI: 10.1088/1674-1056/24/8/087202

Spin transport characteristics modulated by the GeBi interlayer in $Y_3Fe_5O_{12}$/GeBi/Pt heterostructures

Mingming Li(李明明)[1], Lei Zhang(张磊)[2], Lichuan Jin(金立川)[2], and Haizhong Guo(郭海中)[1,3,†]

[1] *Key Laboratory of Materials Physics, Ministry of Education, School of Physics and Microelectronics, Zhengzhou University, Zhengzhou* 450052, *China*
[2] *State Key Laboratory of Electronic Thin Films & Integrated Devices, University of Electronic Science and Technology of China, Chengdu* 610054, *China*
[3] *Institute of Quantum Materials and Physics, Henan Academy of Sciences, Zhengzhou* 450046, *China*

(Received 7 May 2023; revised manuscript received 30 June 2023; accepted manuscript online 3 July 2023)

For the past few years, germanium-based semiconductor spintronics has attracted considerable interest due to its potential for integration into mainstream semiconductor technology. The main challenges in the development of modern semiconductor spintronics are the generation, detection, and manipulation of spin currents. Here, the transport characteristics of a spin current generated by spin pumping through a GeBi semiconductor barrier in $Y_3Fe_5O_{12}$/GeBi/Pt heterostructures were investigated systematically. The effective spin-mixing conductance and inverse spin Hall voltage to quantitatively describe the spin transport characteristics were extracted. The spin-injection efficiency in the $Y_3Fe_5O_{12}$/GeBi/Pt heterostructures is comparable to that of the $Y_3Fe_5O_{12}$/Pt bilayer, and the inverse spin Hall voltage exponential decays with the increase in the barrier thickness. Furthermore, the band gap of the GeBi layer was tuned by changing the Bi content. The spin-injection efficiency at the YIG/semiconductor interface and the spin transportation within the semiconductor barrier are related to the band gap of the GeBi layer. Our results may be used as guidelines for the fabrication of efficient spin transmission structures and may lead to further studies on the impacts of different kinds of barrier materials.

Keywords: spin current, $Y_3Fe_5O_{12}$/GeBi/Pt heterostructures, spin pumping, inverse spin Hall effect

PACS: 72.25.Mk, 76.50.+g, 67.30.hj **DOI:** 10.1088/1674-1056/ace3aa

For the past few years, germanium-based semiconductor spintronics has attracted considerable interest because of its potential for integration into mainstream semiconductor technology.[1,2] The main challenges in the development of modern semiconductor spintronics are the generation, detection, and manipulation of spin currents.[3–10] The manipulation of a pure spin current results in low-cost energy and high-efficiency electronics. Compared with the traditional spin-injection method that introduces a spin-polarized charge current,[11–15] in a ferromagnet (FM)/nonmagnetic (NM) material structure, ferromagnetic resonance (FMR)-driven spin pumping can generate a pure spin current without a charge current via the angular momentum transfer from FM to NM material.[16–20] This dynamic coupling process is generally understood as the exchange interaction between the precessing magnetization of the ferromagnet and the conduction electrons of the normal metal at the interface region.[21,22]

Inverse spin Hall effect (ISHE) measurements are widely employed to detect the change in the spin current from the extracted dc inverse spin Hall voltage. The efficiency of spin pumping is quantified by the spin-mixing conductance parameter.[23] Modulation of spin transport in semiconductors and the fabrication of advanced spintronic devices have always been the focus of semiconductor spintronics research. Cerqueira *et al.* reported the important role played by the localized states at the MgO–Si interface for the generation of spin currents in hybrid metal–silicon–metal vertical structures.[4] Kalappattil *et al.* reported an enhancement in the spin current through an interface organic semiconductor in a $Y_3Fe_5O_{12}$ (YIG)/C_{60}/Pt heterostructure. The presence of C_{60} not only decreases the conductivity mismatch between YIG and Pt, but also reduces the surface perpendicular magnetic anisotropy of YIG.[24] However, the underlying mechanism of spin-current transmission in semiconductors is not fully understood and needs further clarification.

By considering the integration of spintronic devices into traditional semiconductor mainstream technology, we have fabricated a series of $Ge_{1-x}Bi_x$ ($x = 0.04$, 0.07, 0.11, and 0.15) films and investigated the transport characteristics of the spin current in $Y_3Fe_5O_{12}$/GeBi/Pt heterostructures. The extracted inverse spin Hall voltage shows an exponential decay with the increase in the semiconductor barrier thickness. Different Bi concentrations could be used to tune the band gap and the spin decay length of GeBi films. Furthermore, the spin-injection efficiency is also dependent on the band gap of the GeBi barrier. Our results will provide an efficient method to improve the spin-injection efficiency in semiconductor materials.

High-quality YIG single-crystal films were epitaxially grown on (111) $Gd_3Ga_5O_{12}$ substrates with a thickness of 200 nm by liquid phase epitaxy. The $Ge_{1-x}Bi_x$ films were deposited using molecular beam epitaxy at a basic vacuum pressure of 4×10^{-9} Torr. The Ge source temperature was fixed at 1200 °C. The Bi source temperatures were maintained at 425 °C, 450 °C, 475 °C, and 485 °C, and the correspond-

†Corresponding author. E-mail: hguo@zzu.edu.cn

© 2024 Chinese Physical Society and IOP Publishing Ltd

ing Bi concentrations were 4%, 7%, 11%, and 15%. During the growth of GeBi films, the substrate temperature was maintained at 150 °C to allow Bi atom incorporation in the Ge lattices without Bi precipitation or agglomeration. Figure 1(a) shows the x-ray photoelectron spectroscopy (XPS) full spectrum of GeBi films. The main elements are found to be Ge, Bi, and C. The presence of carbon (C) is inevitable and was used for data calibration. Moreover, the element proportion of the film was determined by fitting the peak area of Bi 4f and Ge 3d. The phase formation of GeBi films with different Bi content was characterized by x-ray diffraction (XRD), as shown in Fig. 1(b). There are two diffraction peaks corresponding to GeBi along the (012) direction around 27.1° and the (104) direction around 38.2°. It is well known that the atomic radius of Bi is bigger than that of Ge. When the content of Bi increased from 4% to 15%, the diffraction peak of GeBi moved towards a lower diffraction angle, which means the Bi atom was incorporated into the Ge lattice. The transmission electron microscopy (TEM) results of the interfacial region in the YIG/$Ge_{0.85}Bi_{0.15}$ bilayer are shown in Fig. 1(c). It is observed that the interface is atomically sharp. Figure 1(d) shows the distribution of Fe, Ge, and Bi elements at the interface region. There is no element diffusion at the interface.

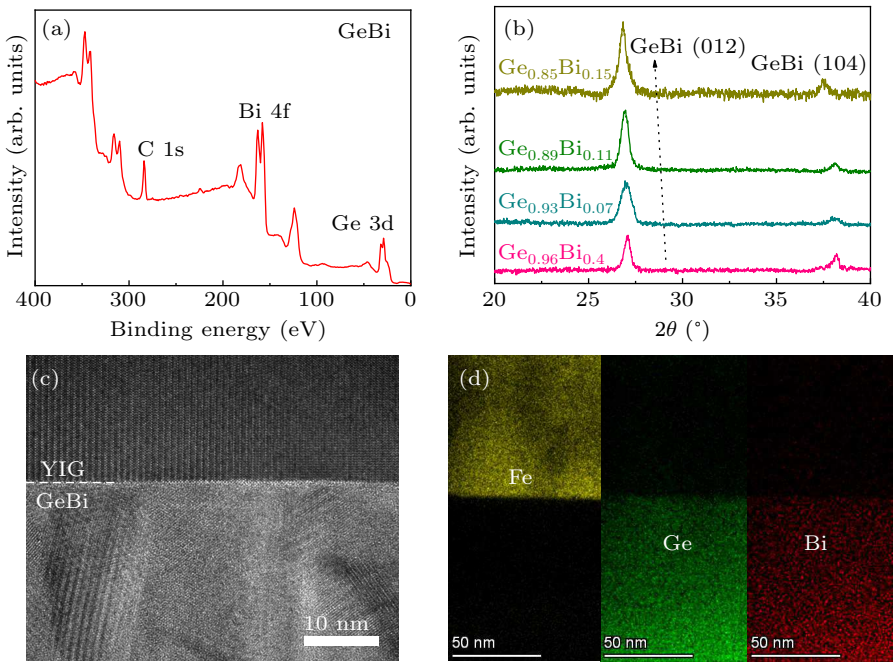


Fig. 1. The XPS, XRD and TEM results of GeBi (100 nm) in the YIG/GeBi bilayer. (a) The XPS full spectrum of $Ge_{0.85}Bi_{0.15}$ in the YIG/$Ge_{0.85}Bi_{0.15}$ bilayer. (b) The XRD scans of GeBi films with different Bi contents. (c) The TEM image of the interfacial region in the YIG/$Ge_{0.85}Bi_{0.15}$ bilayer. (d) The distribution of Fe, Ge, and Bi elements at the interface region.

We investigated the spin-pumping efficiency of the $Y_3Fe_5O_{12}$/GeBi/Pt heterostructures using a wideband ferromagnetic resonance (FMR) system. The microwave power was fixed at 10 dBm to avoid the influence of nonlinear effects that may appear under high power. The microwave frequency ranged from 2 GHz to 15 GHz to ensure the reliability of our data fitting. The FMR measurements were carried out using a coplanar waveguide (CPW) at room temperature with in-plane field sweeping. The magnetization dynamics of YIG can be described by the Landau–Lifshitz–Gilbert equation[23]

$$\frac{\partial \boldsymbol{M}}{\partial t} = -\gamma[\boldsymbol{M} \times \boldsymbol{H}_{\text{eff}}] + \alpha \left[\boldsymbol{M} \times \frac{\partial \boldsymbol{n}}{\partial t}\right], \tag{1}$$

where $\boldsymbol{M}$ is the magnetization vector of M_s and $\boldsymbol{n}$ is the unit vector parallel to $\boldsymbol{M}$. Here, γ is the gyromagnetic ratio, $\boldsymbol{H}_{\text{eff}}$ is the sum of internal and external H fields and α is the Gilbert damping constant. In these conditions, the spin current is generated at the YIG/GeBi interface, while the precessing magnetization of YIG acts as a peristaltic spin pump. This results in dynamic spin accumulation diffusing away from the interface. Moreover, the generation of a spin current is directly reflected as damping enhancement of YIG. We measured the FMR linewidth (ΔH) as a function of the microwave frequency (f) of bare YIG, YIG/Pt and YIG/$Ge_{1-x}Bi_x$/Pt samples, as shown in Fig. 2(a) and fitted according to[25–28]

$$\Delta H = \frac{4\pi\alpha f}{\gamma} + \Delta H_0, \tag{2}$$

where ΔH_0 is the inhomogeneous broadening, independent of the resonance frequency. The thicknesses of the $Ge_{1-x}Bi_x$ and Pt layers are 0.5 nm and 10 nm, respectively. It is worth noting that the FMR linewidth of YIG increased significantly after the capper of Pt and GeBi at the same microwave frequency, which means that the injection of the spin current took place through the interface. We calculated the effective spin-mixing conductance ($g_{\text{eff}}^{\uparrow\downarrow}$) quantitatively to describe the spin-injection

efficiency using[29,30]

$$g_{\text{eff}}^{\uparrow\downarrow} = \frac{4\pi M_s t_{\text{YIG}}}{g\mu_{\text{B}}} \left(\alpha_{\text{YIG/GeBi/Pt}} - \alpha_{\text{YIG}}\right), \tag{3}$$

where g, μ_{B}, and t_{YIG} represent the Lande factor, the Bohr magneton, and the thickness of the YIG layer, respectively. The damping constant for bare YIG (α_{YIG}) is 1.1×10^{-4}. The calculated effective damping constant and effective spin-mixing conductance are shown in Fig. 2(b). The damping constant increases gradually to 5.6×10^{-4} in the YIG/$Ge_{1-x}Bi_x$/Pt samples when the Bi content reaches 15% ($x = 0.15$). The effective spin-mixing conductance also shows similar trends. The spin-injection efficiency is about three times when the Bi content increases from 4% to 15%. Low spin-injection efficiency has always been the main factor that limits the applications of semiconductor spintronic devices. The effective spin-mixing conductance in YIG/$Ge_{0.85}Bi_{0.15}$/Pt is 8.3×10^{18} m^{-2}, which is close to that in YIG/Pt (9.2×10^{18} m^{-2}). We achieved efficient spin injection at the FM/semiconductor interface by tuning the doping content of Bi in the GeBi films.

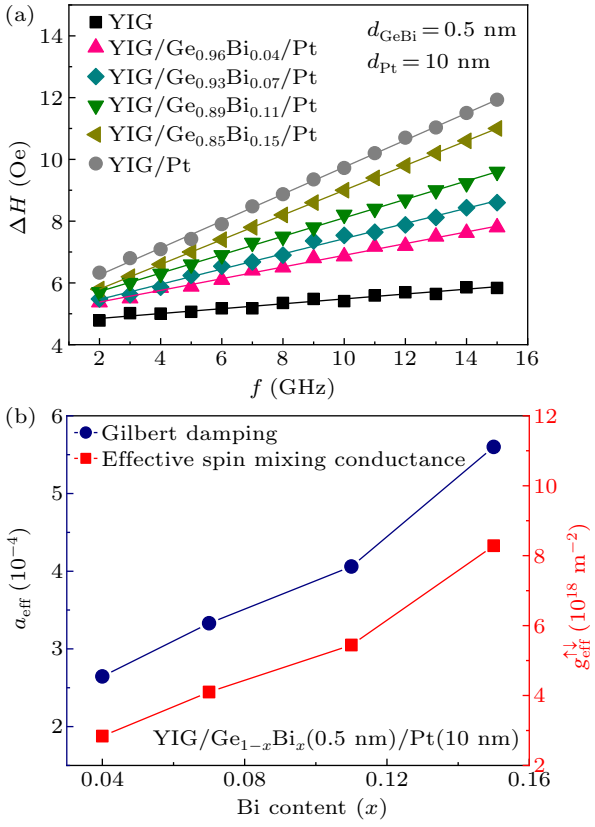


Fig. 2. (a) The FMR linewidth as a function of the microwave frequency of bare YIG, YIG/Pt and YIG/$Ge_{1-x}Bi_x$/Pt samples. (b) The calculated effective damping constant and effective spin-mixing conductance of YIG/$Ge_{1-x}Bi_x$/Pt samples.

The inverse spin Hall effect directly reflects the amount of spin current injected into the Pt layer and is easy to measure. Normal metal like Pt has strong spin–orbit coupling and a large spin Hall angle (θ_{SH}), in which the pumped spin current is converted into a DC charge current by the inverse spin Hall effect. To determine the underlying mechanisms in the spin transport characteristics in the GeBi semiconductor, we measured the inverse spin Hall effect of the YIG/$Ge_{1-x}Bi_x$/Pt samples. Figure 3(a) shows a schematic of the inverse spin Hall effect measurement setup. Similar to the FMR measurements, the inverse spin Hall voltage (V_{ISHE}) was measured at room temperature with in-plane field sweeping. The rf field h_{rf} is perpendicular to the coplanar waveguide signal line. Here, θ_H is the angle between the external magnetic field H and the measured V_{ISHE}. When $\theta_H = 90°$ the measured inverse spin Hall voltage can be expressed as[22,31,32]

$$V_{\text{ISHE}} = e\frac{\rho}{d}\theta_{\text{SH}} w \lambda_{\text{SD}} \tanh\left(\frac{d}{2\lambda_{\text{SD}}}\right) g_{\text{eff}}^{\uparrow\downarrow} f P \sin^2\theta, \tag{4}$$

where e is the electron charge, and ρ, w and λ_{SD} are the resistivity of the Pt layer, the spin Hall angle, the CPW signal line width and the spin diffusion length, respectively. Here, d is the thickness of the Pt layer, which is fixed at 10 nm; θ is the magnetization precession cone angle, as shown in Fig. 3(a); and P is the ellipticity correction factor arising from the ellipticity of the magnetization precession. The microwave frequency and power were set at 5 GHz and 10 dBm, respectively. Figure 3(b) shows the measured V_{ISHE} around the resonance field of the YIG/$Ge_{0.85}Bi_{0.15}$ (0.5 nm)/Pt (10 nm) sample. The measured voltage curves are Lorentz symmetric, and we also reversed the magnetic field to avoid interference from thermal effects. We also studied the effects of the Bi content on the inverse spin Hall voltage, as shown in Fig. 3(c). The V_{ISHE} increases almost linearly when the Bi content increases from 4% to 15% in GeBi films. We investigated the spin transport characteristics through the GeBi layer by changing the thickness of the GeBi barrier layer. We measured the inverse spin Hall voltage as a function of the $Ge_{1-x}Bi_x$ thickness, which ranges from 0.5 nm to 4 nm, as shown in Fig. 4(d), and the curves here are the fitting results using the following function (5). For a given Bi content, the inverse spin Hall voltage decays exponentially with the increase in the GeBi thickness.

To establish the exponential decay model of the spin current in the semiconductor layer, we introduced the parameter decay length (λ). The inverse spin Hall voltage as a function of the GeBi thickness (d_{GeBi}) is expressed as

$$V_{\text{ISHE}} = V_{\text{ISHE}}\left(d_{\text{GeBi}} = 0\right) \mathrm{e}^{-d_{\text{GeBi}}/\lambda}, \tag{5}$$

where V_{ISHE} ($d_{\text{GeBi}} = 0$) is the inverse spin Hall voltage of the YIG/Pt sample. The fitted decay length parameters as a function of the Bi content are shown in Fig. 4(a). The Bi content shows a strong modulation effect on the decay length, i.e., the spin transmission characteristics within the semiconductor barrier. We obtained a decay length of 1.98 nm in $Ge_{0.85}Bi_{0.15}$; however, the decay length reduces to 0.80 nm in $Ge_{0.96}Bi_{0.04}$. A higher Bi content is favorable for spin transport in GeBi

films. Combined with the results of the above spin-pumping measurements, we found that both the calculated spin decay length and effective spin-mixing conductance increased with the Bi content. Figure 4(b) further shows the relationship between the spin decay length and damping enhancement, which indicates that the spin transfer inside the semiconductor is also related to the spin injection through the YIG/semiconductor interface.

When we consider the characteristics of the spin-pumping mode and the YIG's insulating properties, the spin current in the YIG/GeBi/Pt structures is expected to come from the exchange interaction between the conduction electrons of Pt and the processing magnetization of YIG. Thus, the spin transport characteristics are sensitive to the band gap of the

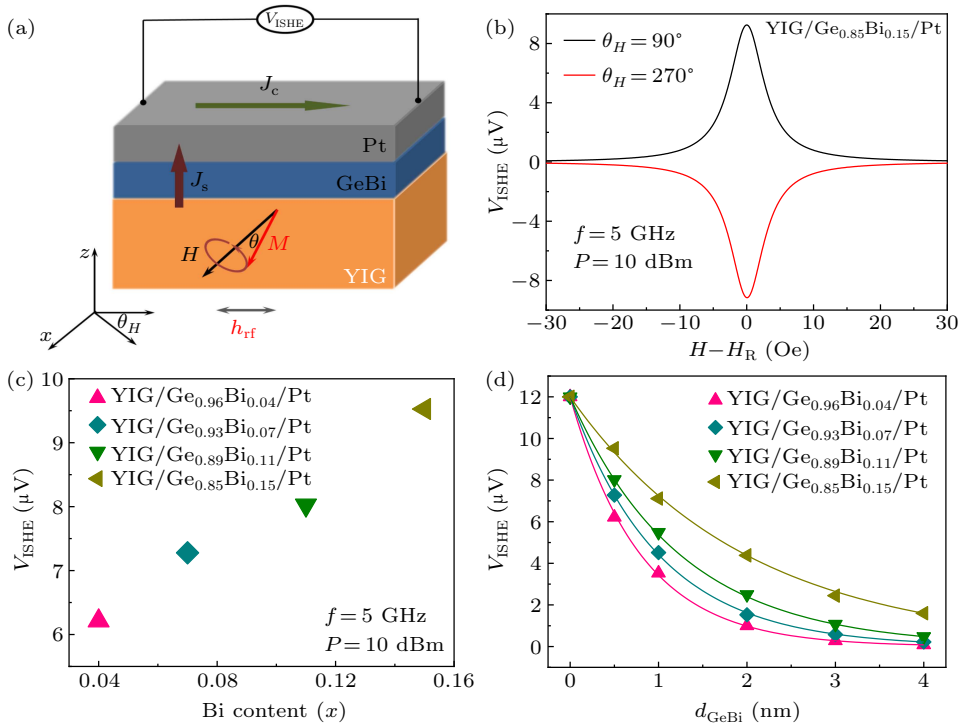


Fig. 3. (a) A schematic of the inverse spin Hall effect measurement. (b) The V_{ISHE} around the resonance field of the YIG/$Ge_{0.85}Bi_{0.15}$ (0.5 nm)/Pt (10 nm) sample. (c) The V_{ISHE} as a function of the Bi content in YIG/$Ge_{1-x}Bi_x$/Pt samples, and (d) the V_{ISHE} as a function of the $Ge_{1-x}Bi_x$ barrier thickness.

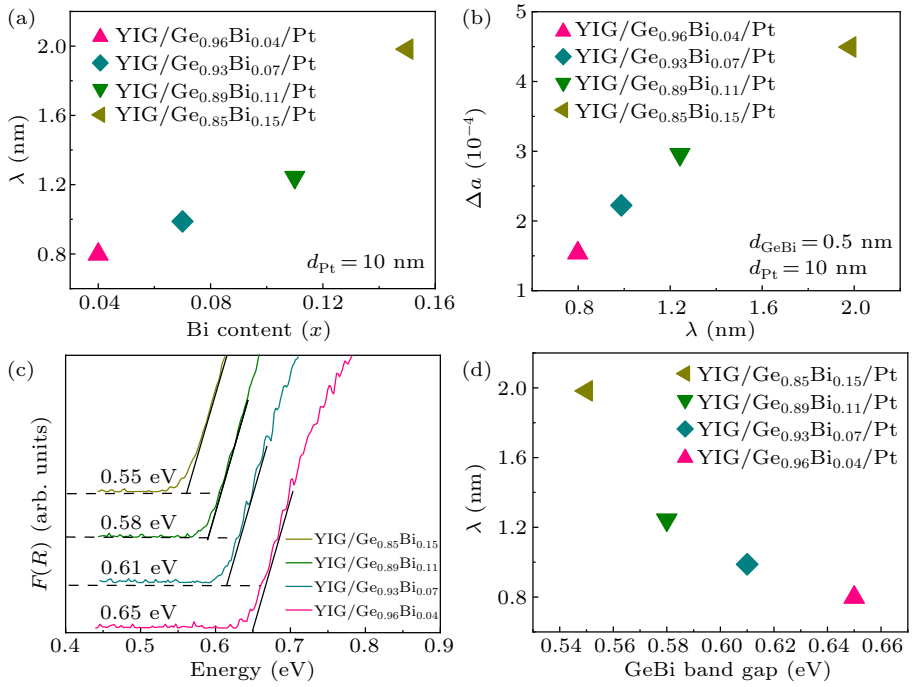


Fig. 4. (a) The fitted spin decay length as a function of the Bi content. (b) The relationship between the spin decay length and damping enhancement. (c) The absorption spectra of $Ge_{1-x}Bi_x$ film. (d) The spin decay length as a function of the band gap in YIG/$Ge_{1-x}Bi_x$/Pt structures.

semiconductor barrier.[33] The near-infrared properties of the YIG/$Ge_{1-x}Bi_x$ samples with different Bi content were used to identify the band gap of the doped semiconductor thin films. The absorption spectra for $Ge_{1-x}Bi_x$ film, as shown in Fig. 4(c), was transformed from the diffuse reflectance (R) spectra using the Kubelka–Munk function[33]

$$F(R) = \frac{(1-R)^2}{2R}. \tag{6}$$

The band gap was extracted at the intersection of the linear fit and photon energy axis. The enhancement of doped Bi causes a decrease in the band-gap of $Ge_{1-x}Bi_x$ films, which is similar to the results presented in a previous study of GeSn, another Ge-based semiconductor.[34] The band gap of $Ge_{0.96}Bi_{0.04}$ is found to be 0.65 eV and subsequently reduced to 0.55 eV in $Ge_{0.85}Bi_{0.15}$ films. Figure 4(d) shows the spin decay length as a function of the band gap in the YIG/$Ge_{1-x}Bi_x$/Pt structures. The smaller barrier band gap corresponds to the longer spin decay length. Furthermore, one may notice that both the characteristics of spin transfer inside the semiconductor (Fig. 4(a)) and the spin injection through the interface (Fig. 4(b)) for $Ge_{0.85}Bi_{0.15}$ have more significant changes compared to those with low Bi content (4% to 11%). This may be due to the change in the band-gap type. Ge itself is an indirect band gap semiconductor and gets converted into a direct band-gap material when the Sn doping reaches a certain doping concentration.[35] A similar transformation might have occurred in the GeBi films.

In conclusion, we manipulated the band gap of $Ge_{1-x}Bi_x$ films by changing the doping concentration of Bi and investigated the spin transport characteristics in YIG/$Ge_{1-x}Bi_x$/Pt structures. The spin current through the semiconductor barrier showed an exponential decay with the increase in the barrier thickness. The spin-injection efficiency at the YIG/$Ge_{1-x}Bi_x$ interface increased with the Bi content. We identified the band gap of $Ge_{1-x}Bi_x$ films and found that the band gap of the semiconductor barrier plays an important role in the spin-injection efficiency through the YIG/semiconductor interface and also the transportation within the semiconductor barrier. Our findings provide a method to improve spin-injection efficiency at the FM/semiconductor interface and offer potential guidance for the combination of mainstream semiconductor technology and spintronics.

Acknowledgments

Project supported by the National Key Research and Development Program of China (Grant No. 2021YFA0718701), the China Postdoctoral Science Foundation (Grant No. 2022M722888), and the National Natural Science Foundation of China (Grant Nos. 12174347 and 12004340).

References

[1] Jain A, Rojas-Sanchez J C, Cubukcu M, *et al.* 2012 *Phys. Rev. Lett.* **109** 106603
[2] Dushenko S, Koike M, Ando Y, Shinjo T, Myronov M and Shiraishi M 2015 *Phys. Rev. Lett.* **114** 196602
[3] Appelbaum I, Huang B and Monsma D 2007 *Nature* **447** 295
[4] Cerqueira C, Qin J Y, Dang H, *et al.* 2019 *Nano Lett.* **19** 90
[5] Pu Y, Odenthal P M, Adur R, Beardsley J, Swartz A G, Pelekhov D V, Flatté M E, Kawakami R K, Pelz J, Hammel P C and Johnston-Halperin E 2015 *Phys. Rev. Lett.* **115** 246602
[6] Xie H F, Chang Y H, Guo X, Zhang J R, Cui B S, Zuo Y L and Xi L 2023 *Chin. Phys. B* **32** 037502
[7] Lou P C, Katailiha A, Bhardwaj R G, Bhowmick T, Beyermann W P, Lake R K and Kumar S 2020 *Phys. Rev. B* **101** 094435
[8] Ando K and Saitoh E 2012 *Nat. Commun.* **3** 629
[9] Ezhevskii A A, Guseinov D V, Soukhorukov A V, Novikov A V, Yurasov D V and Gusev N S 2020 *Phys. Rev. B* **101** 195202
[10] Kato Y K, Myers R C, Gossard A C and Awschalom D D 2004 *Science* **306** 1910
[11] Niimi Y, Morota M, Wei D H, Deranlot C, Basletic M, Hamzic A, Fert A and Otani Y 2011 *Phys. Rev. Lett.* **106** 126601
[12] Huang Z C, Liu W Q, Liang J, Guo Q J, Zhai Y and Xu Y B 2022 *Chin. Phys. B* **31** 068505
[13] Yuan S P, Shen C, Zheng H Z, Liu Q, Wang L G, Meng K K and Zhao J H 2013 *Chin. Phys. B* **22** 047202
[14] Niimi Y, Kawanishi Y, Wei D H, Deranlot C, Yang H X, Chshiev M, Valet T, Fert A and Otani Y 2012 *Phys. Rev. Lett.* **109** 156602
[15] Yan W, Sagasta E, Ribeiro M, Niimi Y, Hueso L E and Casanova F 2017 *Nat. Commun.* **8** 661
[16] Wang Y, Decker M M, Meier T N G, Chen X, Song C, Grünbaum T, Zhao W, Zhang J, Chen L and Back C H 2020 *Nat. Commun.* **11** 275
[17] Safi T S, Zhang P, Fan Y, Guo Z, Han J, Rosenberg E R, Ross C, Tserkovnyak Y and Liu L 2020 *Nat. Commun.* **11** 476
[18] Mosendz O, Pearson J E, Fradin F Y, Bauer G E W, Bader S D and Hoffmann A 2010 *Phys. Rev. Lett.* **104** 046601
[19] Tserkovnyak Y, Brataas A and Bauer G E W 2002 *Phys. Rev. B* **66** 224403
[20] Rojas-Sánchez J C, Reyren N, Laczkowski P, Savero W, Attané J P, Deranlot C, Jamet M, George J M, Vila L and Jaffrès H 2014 *Phys. Rev. Lett.* **112** 106602
[21] Tserkovnyak Y, Brataas A and Bauer G E W 2002 *Phys. Rev. Lett.* **88** 117601
[22] Kajiwara Y, Harii K, Takahashi S, *et al.* 2010 *Nature* **464** 262
[23] Montoya E, Omelchenko P, Coutts C, Lee-Hone N R, Hübner R, Broun D, Heinrich B and Girt E 2016 *Phys. Rev. B* **94** 054416
[24] Kalappattil V, Geng R, Das R, *et al.* 2020 *Mater. Horiz.* **7** 1413
[25] Wang H L, Du C H, Hammel P C and Yang F Y 2014 *Appl. Phys. Lett.* **104** 202405
[26] Wang L, Jing Z X, Zhou A R and Li S D 2022 *Chin. Phys. B* **31** 086201
[27] Jungfleisch M B, Chumak A V, Kehlberger A, Lauer V, Kim D H, Onbasli M C, Ross C A, Kläui M and Hillebrands B 2015 *Phys. Rev. B* **91** 134407
[28] Omelchenko P, Girt E and Heinrich B 2019 *Phys. Rev. B* **100** 144418
[29] Wang H L, Du C H, Pu Y, Adur R, Hammel P C and Yang F Y 2014 *Phys. Rev. Lett.* **112** 197201
[30] Tserkovnyak Y, Brataas A and Bauer G E W 2002 *Phys. Rev. Lett.* **88** 117601
[31] Du C H, Wang H L, Yang F Y and Hammel P C 2014 *Phys. Rev. B* **90** 140407
[32] Li M M, Jin L C, Zhong Z Y, Tang X L, Yang Q H, Zhang L and Zhang H W 2020 *Phys. Rev. B* **102** 174435
[33] Du C H, Wang H L, Pu Y, Meyer T L, Woodward P M, Yang F Y and Hammel P C 2013 *Phys. Rev. Lett.* **111** 247202
[34] Gassenq A, Milord L, Aubin J, Guilloy K, Tardif S, Pauc N, Rothman J, Chelnokov A, Hartmann J M, Reboud V and Calvo V 2016 *Appl. Phys. Lett.* **109** 242107
[35] Wirths S, Geiger R, Driesch N, Mussler G, Stoica T, Mantl S, Ikonic Z, Luysberg M, Chiussi S, Hartmann J M, Sigg H, Faist J, Buca D and Grützmacher D 2015 *Nat. Photon.* **9** 88